Electronic Supplementary Information

Encapsulated RuP_2-RuS_2 nanoheterostructure with regulated interfacial charge redistribution for synergistically boosting hydrogen evolution electrocatalysis

Ping Li,*[a,b] Wenqin Li,[a,b] Yuqi Huang,[a,b] Jixin Li, [a,b] Quhua Huang, [a,b] Shien Zhao,[a,b] and Shuanghong Tian [a,b]

[a] *School of Environmental Science and Engineering, Sun Yat-sen University, Guangzhou 510275, Guangdong, P. R. China.*

[b] *Guangdong Provincial Key Laboratory of Environmental Pollution Control and Remediation Technology, Guangzhou 510275, PR China.*

E-mail: liping56@mail.sysu.edu.cn

Experimental Section

Materials and reagents

The following chemicals were used as received without any further purification treatment. $RuCl_3 \cdot xH_2O$ (35.0~42.0% Ru basis), ammonium chloride（NH_4Cl, 99.5%), dicyandiamide (DCDA, 99%), hexachlorocyclophosphazene (HCCP, 98%), 4,4'-sulfonyldiphenol (BPS, 99%), triethylamine (TEA, 99%)，thiourea (CH_4N_2S, 99%) and potassium hydroxide (KOH, 85%) were purchased from Aladdin. Ethanol (99.99%), and methanol (MeOH, 99.99%) were purchased from Sinopharm Chemical Reagent Co. Ltd. Perfluorosulfonic acid−poly(tetrafluoroethylene) copolymer (Nafion, 5% w/w in water) was purchased from Sigma-Aldrich. Deionized water was from the Mill Q HX 7040 Purified Water system.

Electrochemical measurements

The electrochemical measurements were carried out using a computer-controlled electrochemical workstation (Autolab, PGSTAT 302N) with a standard three-electrode system, in which a catalyst-modified glassy carbon electrode (GCE, 3 mm in diameter) was used as the working electrode, a graphite rod as the counter electrode, and Hg/HgO (filled with 1.0 M KOH solution) electrode as the reference electrode. The preparation for the working electrode was as follows: solid catalyst (3 mg) was dispersed in 484 μL of water, 120 μL of ethanol, and 31 μL of 5 wt% Nafion solution. After ultrasonicating the mixture for about 30 min, the homogeneous catalyst ink was obtained. Next, 3 μL of catalyst ink was loaded onto the GCE (loading amount about 0.2 mg cm^{-2} for all the samples). Finally, the electrode was dried at room temperature overnight.

In this work, before all the experiments, the electrolyte solution (1.0 M KOH) was purged with N_2 for 30 min, the electrochemical measurements were carried out at least on four working electrodes to check the reproducibility and their average was taken into account. All the current densities were normalized to the geometrical area of the GCE, and all the measured potentials vs. Hg/HgO (1.0 M KOH) were converted to a reversible hydrogen electrode (RHE) scale according to the Nernst equation: $E_{(RHE)} = E_{(Hg/HgO)} + 0.098 + 0.0591 \times pH$.

Before the electrochemical catalytic measurement, all the working electrodes were conducted by a continuous cyclic voltammogram (CV) scan from 0 to - 0.5 V (vs. RHE) for several times at a scan rate of 20 mV s^{-1} until the signals were relatively stabilized. Linear sweep voltammetry (LSV) from 0 to - 0.5 V (vs. RHE) was recorded with a scan rate of 2 mV s^{-1} to obtain the polarization curves. All the polarization curves were corrected with 95% iR-compensation.

Electrochemical impedance spectroscopy (EIS) was performed with frequency from 0.1 to 10^5 Hz with an amplitude voltage of 5 mV, and the measured potential was set at - 0.053V vs. RHE for all the samples.

The long-term stability test was performed by chronopotentiometric (CP) measurement in 1.0 M KOH electrolyte. For the above CP measurement, the RuP_2-RuS_2/NPS-C catalyst-modified GCE was used as the working electrode, and the current density was set at 10 mA cm^{-2}. On the other hand, to collect enough amount of catalyst for XRD characterization, the catalyst was also loaded on the carbon cloth to proceed the CP test.

Materials characterization

The morphologies and structures of the samples were investigated by Scanning Electron Microscopy (SEM, Zeiss Sigma 500 electron microscope) with an energy-dispersive X-ray (EDX) analyzer and Transmission Electron Microscopy (TEM, JEOL JEM-2100F, 200 kV). The elemental composition of the materials was studied via inductively coupled plasma-optical emission spectrometer (ICP-OES) (Avio 500). X-ray photoelectron spectroscopy (XPS) was undertaken using a Thermo ESCALAB 250 X-ray photoelectron spectrometer. The binding energy of the C 1s peak (284.8 eV, C-C bond) was used as the internal standard. The crystal phase analysis was conducted using Bruker D8 Advance system X-ray diffractometer (XRD) with Cu Kα radiation. Fourier transform infrared (FT-IR) spectra were performed on Nicolet iS50 spectrometer (Thermo Fisher, USA).

Computational method

Density functional theory (DFT) calculations were performed with the Vienna ab initio Simulation Package (VASP).[1, 2] The projector-augmented wave (PAW) method and Perdew-Burke-Ernzerhof (PBE) functional exchange-correlation within a generalized gradient approximation (GGA) were adopted.[3] The van der Waals (vdW) interaction was considered with the DFT-D3 force-field approach proposed by Grimme.[4] A cutoff energy of 400 eV was used for the plane-wave basis set. The convergence thresholds for energy and force were set as 1×10^{-4} eV and 0.03 eV $Å^{-1}$, respectively. RuP_2 with the (110) facet exposure and RuS_2 with the (200) facet exposure were modeled in the

calculation. The composite of RuS_2/RuP_2 and RuP_2/RuS_2 model were constructed by adjusting the arrangement among the interface to minimize the lattice mismatch (less than 5%). A vacuum space of at least 15 Å was employed to avoid the interaction between periodic units.

The Gibbs free energies of hydrogen adsorption were calculated by the following equations:

$$\Delta G_{H^*} = \Delta E_{H^*} + \Delta ZPE - T\Delta S = E_{H^*} - E_* - 1/2E_{H_2} + \Delta ZPE - T\Delta S$$

where ΔE_{H^*}, E_{H^*}, E_*, and E_{H_2} are the hydrogen binding energy, the total energy of the H-slab system, the energy of the slab, and the energy of H_2 in gas phase, respectively. ΔZPE is the zero point energy difference between the adsorbed and the gas phase hydrogen, and ΔS is the corresponding entropy change between these two states. According to the previous reports, 0.24 eV value was used to represent the correction of zero point energy and entropy of the hydrogen state.[5, 6]

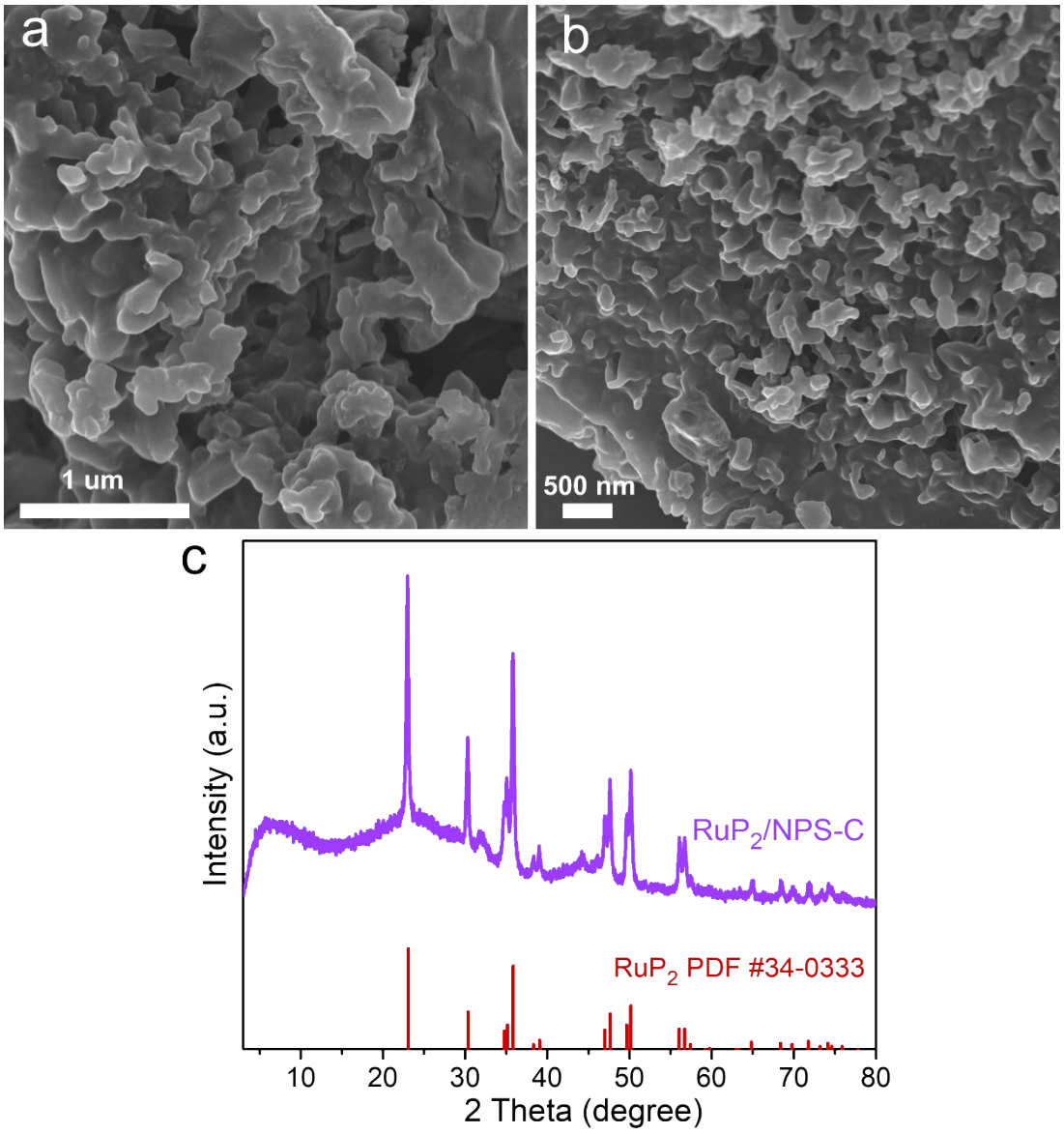

Figure S1. (a,b) SEM images and (c) XRD pattern of the RuP_2/NPS-C.

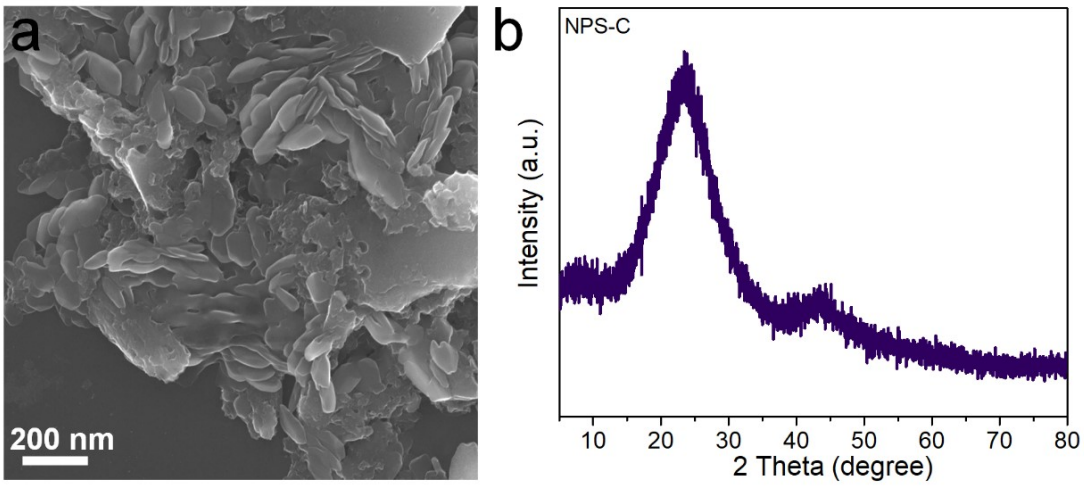

Figure S2. (a) SEM image and (b) XRD pattern of the NPS-C.

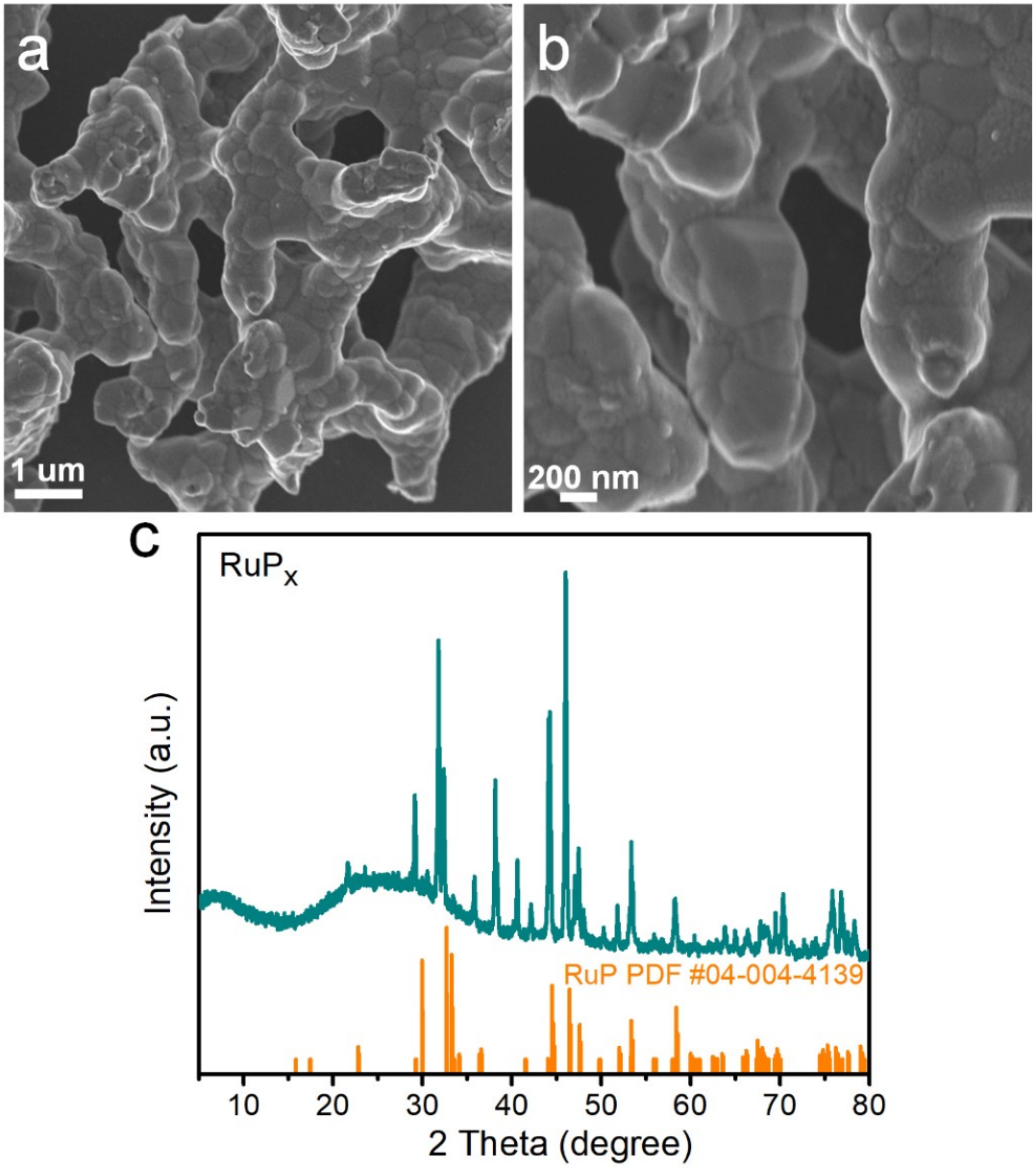

Figure S3. (a,b) SEM images and (c) XRD pattern of the RuP_x.

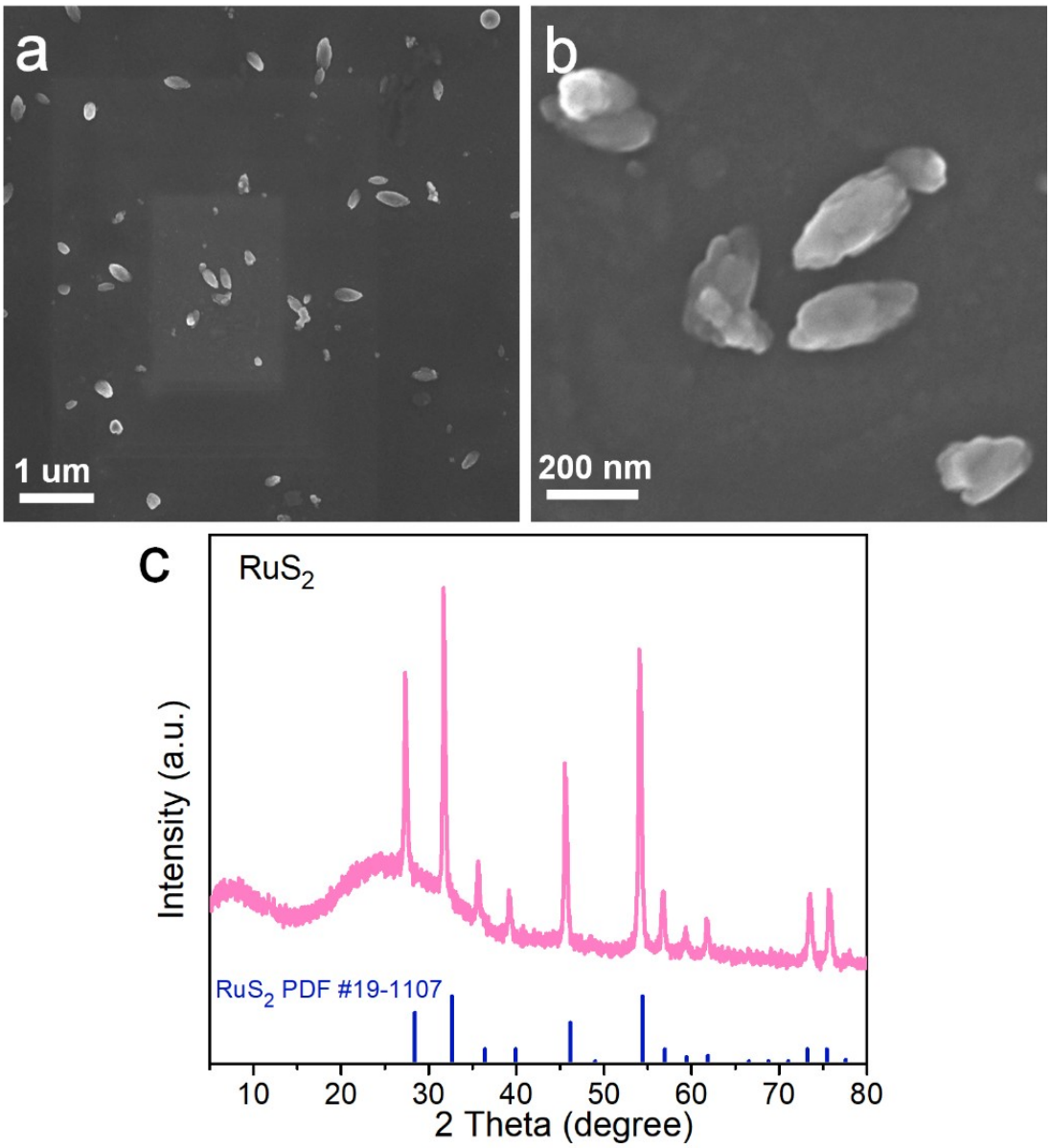

Figure S4. (a,b) SEM images and (c) XRD pattern of the RuS_2.

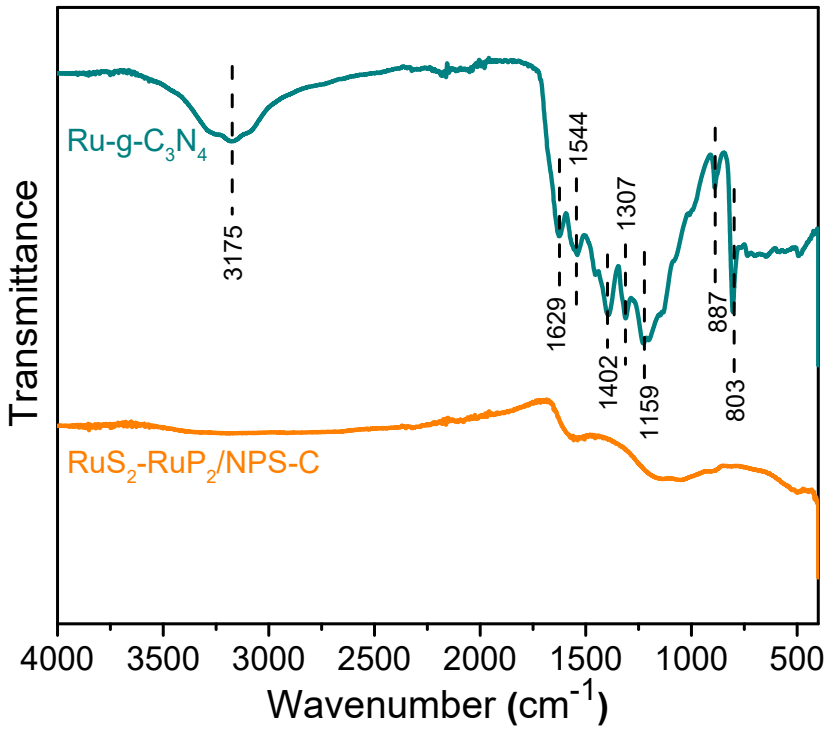

Figure S5. FTIR spectra of the Ru-g-C_3N_4 and RuP_2-RuS_2/NPS-C nanocomposite.

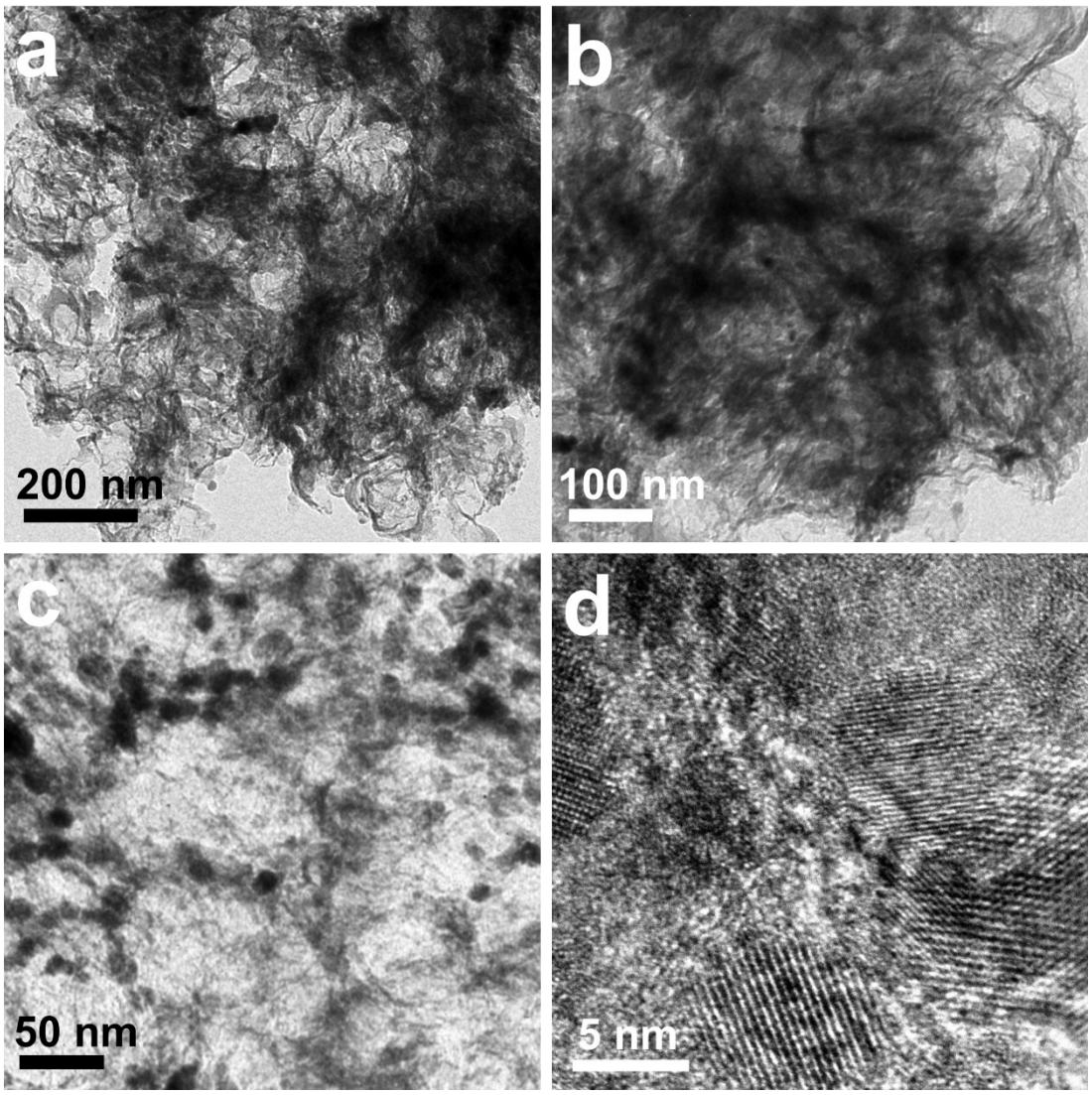

Figure S6. (a-d) TEM images of the RuP_2-RuS_2/NPS-C in different magnifications.

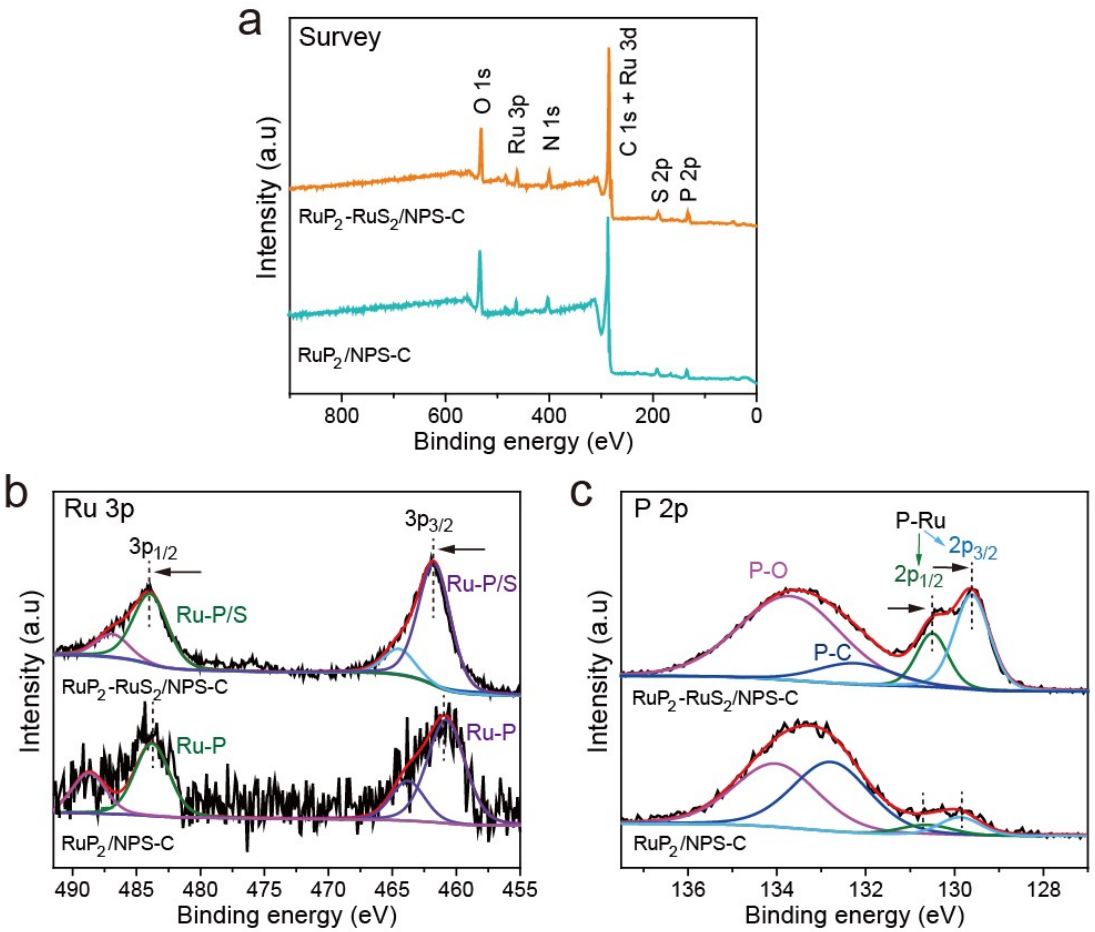

Figure S7. The XPS spectra of the RuP_2/NPS-C nanocomposite: (a) survey spectrum, (b) Ru 3p, and (c) P 2p. The XPS spectra of the RuP_2-RuS_2/NPS-C nanocomposite are also provided for better comparison.

Notes: As demonstrated in Figure S7a, the elements of Ru, P, S, N, and C are present in the XPS survey spectrum, confirming the chemical composition of the RuP_2/NPS-C. Regarding the Ru 3p spectrum shown in Figure S7b, the peaks at 461.5 and 483.7 eV are corresponded to Ru-P species in RuP_2, and the peaks at 464.4 and 488.7 eV can be assigned to Ru-O species. Of note, relative to those of RuP_2/NPS-C, the peaks for Ru-P species in the Ru 3p spectrum of the RuP_2-RuS_2/NPS-C shift to higher binding energy. For the P 2p spectrum shown in Figure S7c, four peaks can be

deconvoluted, the peaks centered at 129.8 and 130.7 eV could be ascribed to P $2p_{3/2}$ and P $2p_{1/2}$ of P−Ru bond, and the peaks at 132.8 and 134.1 eV are consistent with P-C and P-O species, respectively. As depicted, the peaks for P−Ru species in the P 2p spectrum of the RuP_2-RuS_2/NPS-C shift to lower binding energy in comparison with those of RuP_2/NPS-C. The above XPS peak shifts in Ru 3p and P 2p spectra imply that to couple RuS_2 with RuP_2 could lead to the obvious charge redistribution in the form of electron transfer from the Ru atom to P atom, thus electron-deficient Ru sites and electron-rich P sites can be achieved.

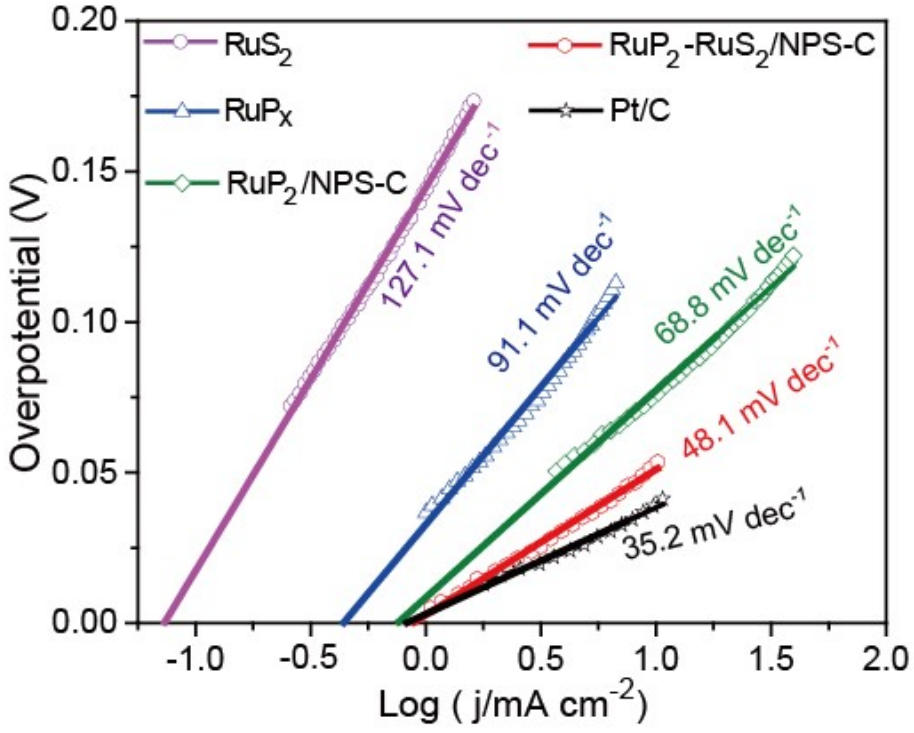

Figure S8. The extrapolated Tafel plots of the RuP_2-RuS_2/NPS-C, RuP_2/NPS-C, RuP_x, RuS_2 and commercial Pt/C catalysts.

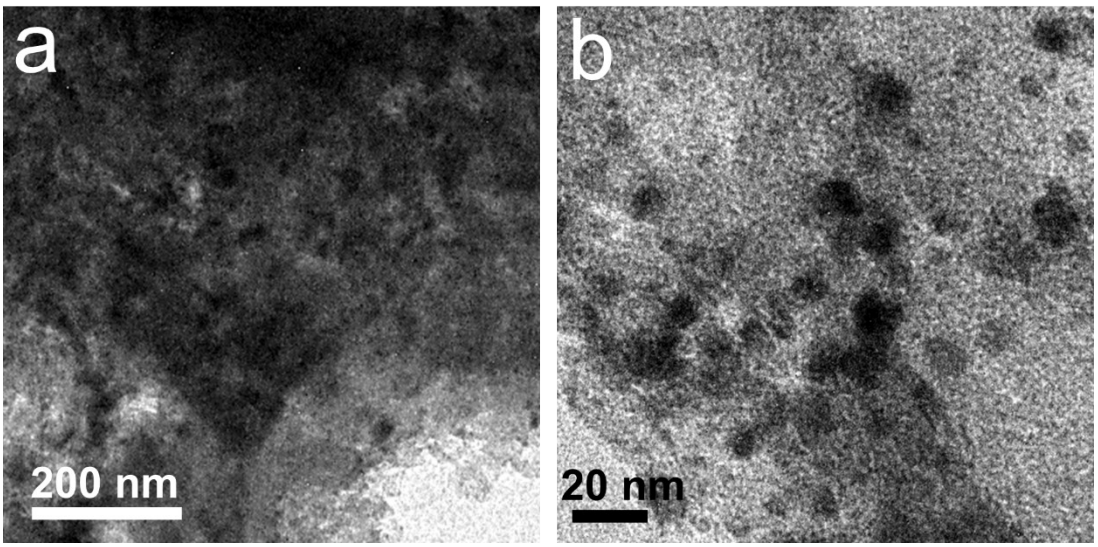

Figure S9. (a,b) TEM images of the used RuP_2-RuS_2/NPS-C nanocomposite after CP stability test.

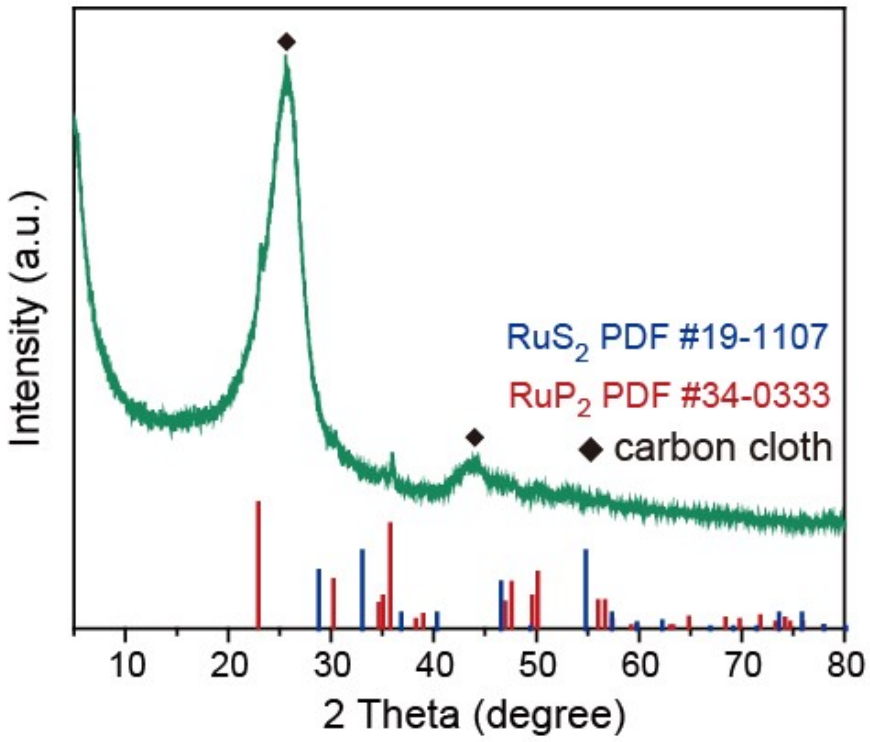

Figure S10. XRD pattern of the used RuP_2-RuS_2/NPS-C nanocomposite after CP stability test.

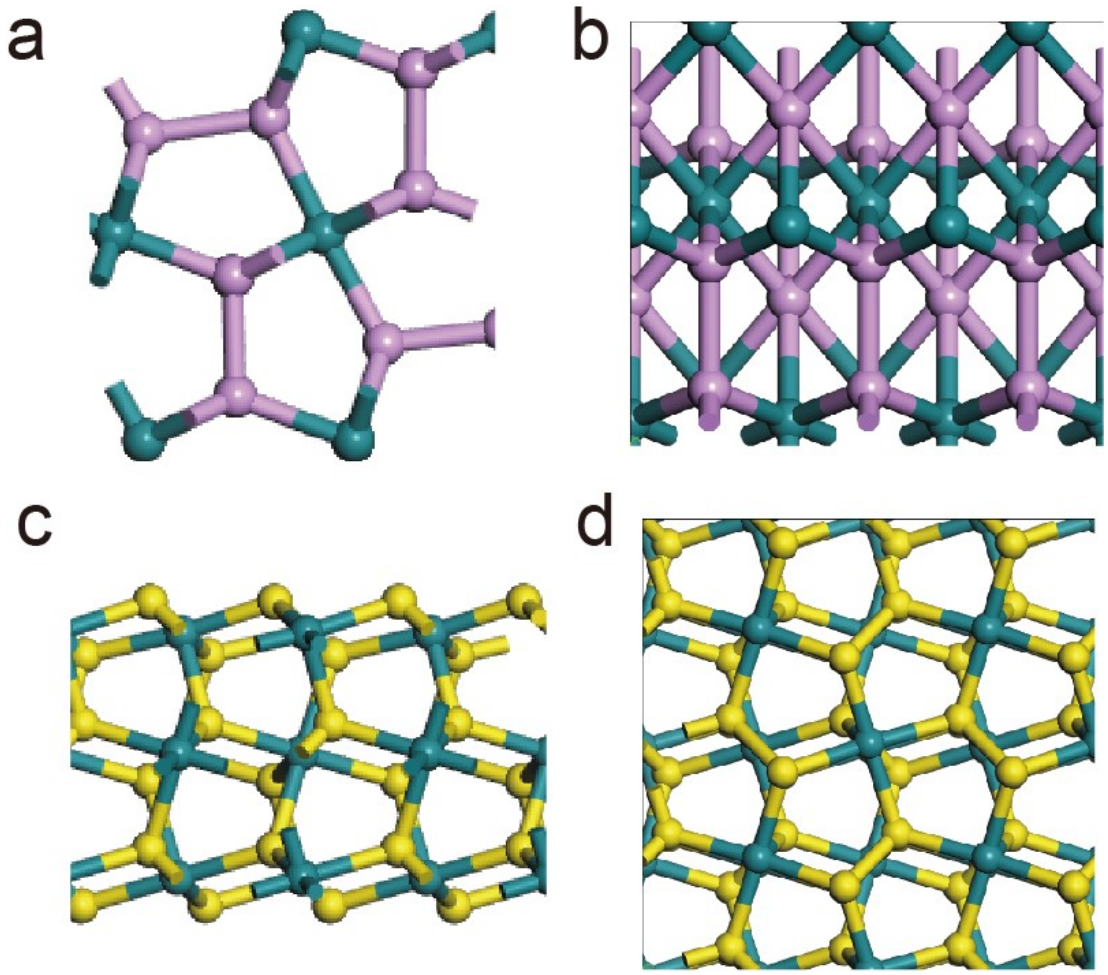

Figure S11. The optimized geometric models for DFT calculations. (a) The side view and (b) top view of the RuP_2 model surface. (c) The side view and (d) top view of the RuS_2 model surface.

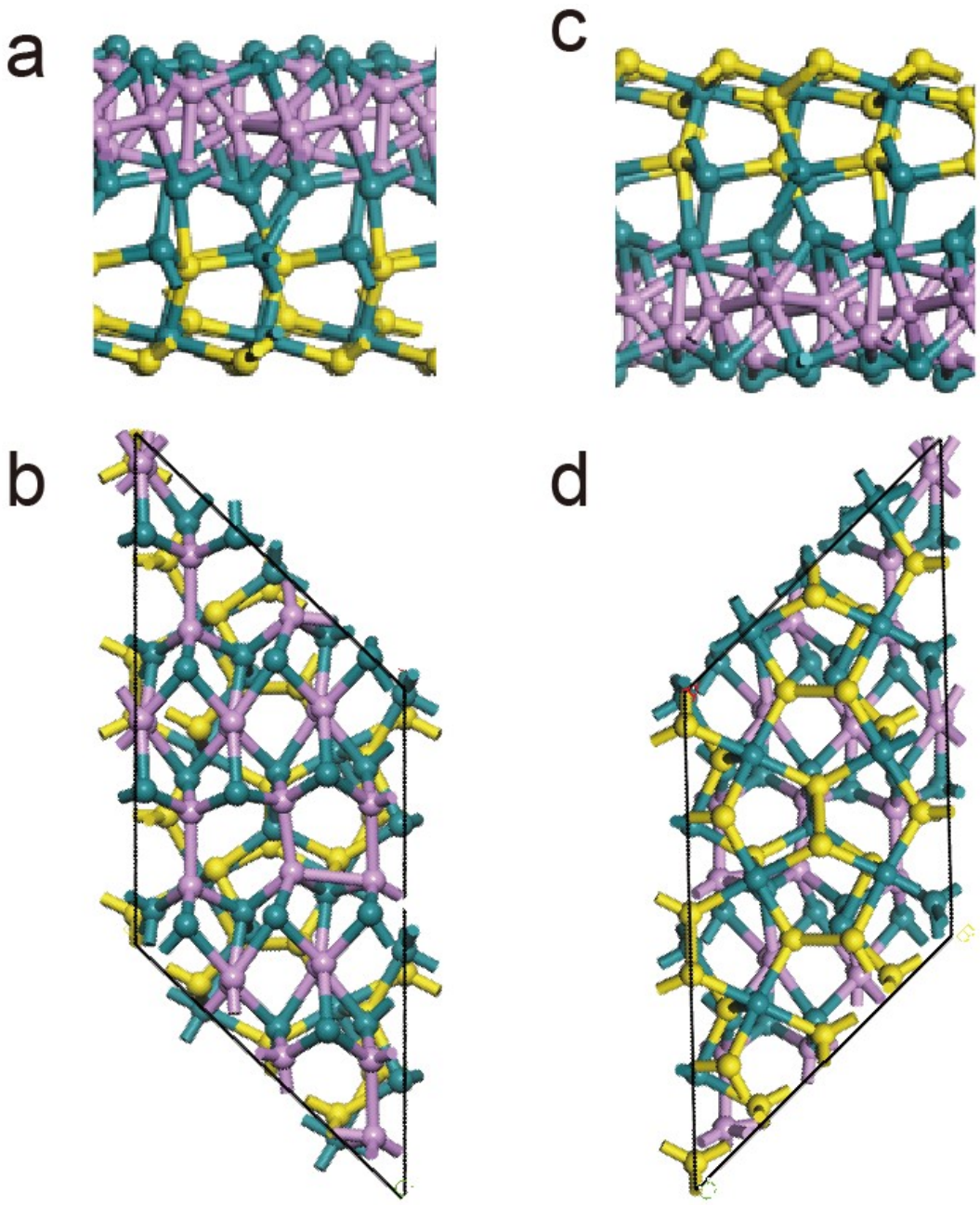

Figure S12. The optimized geometric models for DFT calculations. (a) The side view and (b) top view of the RuP_2/RuS_2 model surface. (c) The side view and (d) top view of the RuS_2/RuP_2 model surface.

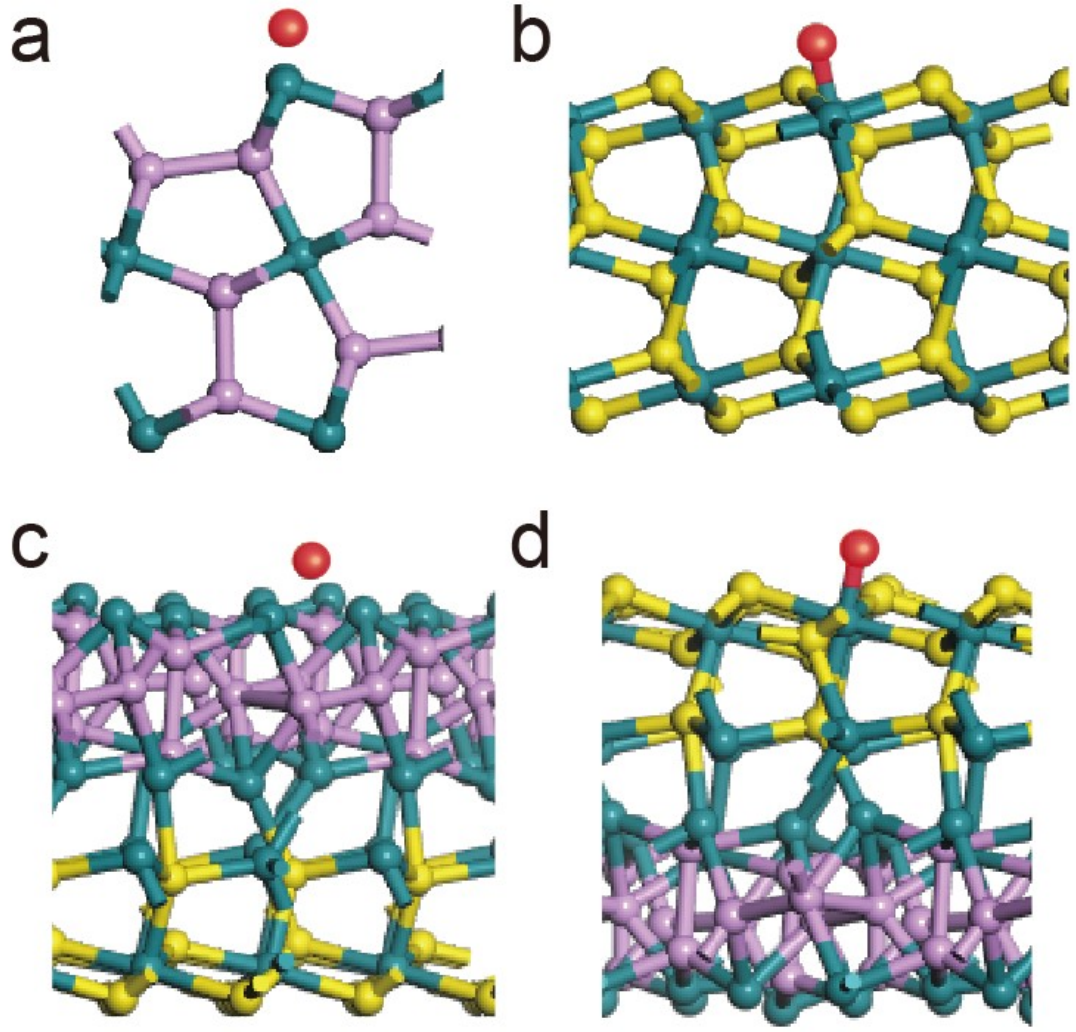

Figure S13. The side view of the optimized structures of the H adsorption on the model surfaces of (a) RuP_2, (b) RuS_2, (c) RuP_2/RuS_2, and (d) RuS_2/RuP_2. The cyan, yellow, pink, and red balls refer to the Ru, S, P, and H atoms, respectively.

Table S1. Comparison of the HER catalytic performance of our RuP_2-RuS_2/NPS-C nanocomposite with other recently reported high-performance HER electrocatalysts in alkaline solution.

Catalyst	Mass loading (mg cm^{-2})	Electrolyte	η@10 mA cm^{-2} (mV)	Tafel slope (mV dec^{-1})	Ref.
RuP_2-RuS_2/NPS-C	0.2	1.0 M KOH	53	48.1	this work
RuPx@NPC	0.2	1.0 M KOH	74	70	7
Ni_5P_4-Ru/CC	N/A	1.0 M KOH	54	52	8
RuP_2@NPC	1.0	1.0 M KOH	52	69	9
R-TiO_2/Ru	0.4	1.0 M KOH	82	97	10
Ru/C	N/A	1.0 M KOH	116	48	11
Ru-Ru_2P	0.38	1.0 M KOH	64	36.7	12
Ru	0.38	1.0 M KOH	72	40.1	
Ru@C_2N	N/A	1.0 M KOH	17	N/A	13
RuP_2 NPs	1	1.0 M KOH	90	73	14
RuP_2-550	0.345	1.0 M KOH	76	74	15
RuCoP	0.3	1.0 M KOH	23	43	16
RuPx/NPC	0.12	1.0 M KOH	74	70	17
CoRu@NC-2	0.27	1.0 M KOH	45	N/A	18
Ru_2P	0.06	1.0 M KOH	57	43	19
RuP	0.06	1.0 M KOH	74	49	
Ni/V_2O_3	N/A	1.0 M KOH	140	112	20
$NiCo_2Px$/CF	5.9	1.0 M KOH	58	34.3	21
$Re_{0.94}Mo_{0.06}Se_2$	N/A	1.0 M KOH	174	112	22
Ni-$ReSe_2$	N/A	1.0 M KOH	109	81	23
NiSe/NF	2.8	1.0 M KOH	96	120	24
CoS_2/SnO_2@MoS_2	0.28	1.0 M KOH	196	69	25
WP_2 NPs/W	N/A	0.5 M KOH 1.0 M KOH	143 214	66 92	26
Ultrathin Ni nanosheets	0.53	1.0 M KOH	80	70	27
Ni-P/CP	N/A	0.5 M KOH 1.0 M KOH	98 117	59 85	28
MoS_2-G-NiO@Ni	N/A	1.0 M KOH	150	80	29
MoP_2 NPs/Mo	N/A	0.5 M KOH 1.0 M KOH	143 194	57 80	30
$Mo_xW_{2-x}C$/N, P-co doped CNTs	0.70	1.0 M KOH	145	73	31

CoP/NC	N/A	0.5 M KOH 1.0 M KOH	78 129	48 58	[32]
Pd−Pt	N/A	1.0 M KOH	71	N/A	[33]

REFERENCES

1. Kresse, G.; Hafner, J. Physical Review B **1993,** 47 (1), 558-561.

2. Kresse, G.; Furthmüller, J. Physical Review B **1996,** 54 (16), 11169-11186.

3. Perdew, J. P.; Burke, K.; Ernzerhof, M. Physical Review Letters **1996,** 77 (18), 3865-3868.

4. Grimme, S.; Antony, J.; Ehrlich, S.; Krieg, H. The Journal of Chemical Physics **2010,** 132 (15), 154104.

5. Nørskov, J. K.; Bligaard, T.; Logadottir, A.; Kitchin, J. R.; Chen, J. G.; Pandelov, S.; Stimming, U. Journal of The Electrochemical Society **2005,** 152 (3), J23.

6. Zheng, Y.; Jiao, Y.; Zhu, Y.; Li, L. H.; Han, Y.; Chen, Y.; Du, A.; Jaroniec, M.; Qiao, S. Z. Nature Communications **2014,** 5 (1), 3783.

7. Chi, J.-Q.; Gao, W.-K.; Lin, J.-H.; Dong, B.; Yan, K.-L.; Qin, J.-F.; Liu, B.; Chai, Y.-M.; Liu, C.-G. ChemSusChem **2018,** 11 (4), 743-752.

8. He, Q.; Tian, D.; Jiang, H.; Cao, D.; Wei, S.; Liu, D.; Song, P.; Lin, Y.; Song, L. Advanced Materials **2020,** 32 (11), 1906972.

9. Pu, Z.; Amiinu, I. S.; Kou, Z.; Li, W.; Mu, S. Angew Chem Int Ed Engl **2017,** 56 (38), 11559-11564.

10. Nong, S.; Dong, W.; Yin, J.; Dong, B.; Lu, Y.; Yuan, X.; Wang, X.; Bu, K.; Chen, M.; Jiang, S.; Liu, L.-M.; Sui, M.; Huang, F. Journal of the American Chemical Society **2018,** 140 (17), 5719-5727.

11. Lu, Q.; Wang, A.-L.; Gong, Y.; Hao, W.; Cheng, H.; Chen, J.; Li, B.; Yang, N.; Niu, W.; Wang, J.; Yu, Y.; Zhang, X.; Chen, Y.; Fan, Z.; Wu, X.-J.; Chen, J.; Luo, J.; Li, S.; Gu, L.; Zhang, H. Nature Chemistry **2018,** 10 (4), 456-461.

12. Yu, J.; Guo, Y.; She, S.; Miao, S.; Ni, M.; Zhou, W.; Liu, M.; Shao, Z. Advanced Materials **2018,** 30 (39), 1800047.

13. Mahmood, J.; Li, F.; Jung, S.-M.; Okyay, M. S.; Ahmad, I.; Kim, S.-J.; Park, N.; Jeong, H. Y.; Baek, J.-B. Nature Nanotechnology **2017,** 12 (5), 441-446.

14. Boppella, R.; Tan, J.; Yang, W.; Moon, J. Advanced Functional Materials **2019,** 29 (6), 1807976.

15. Chang, Q.; Ma, J.; Zhu, Y.; Li, Z.; Xu, D.; Duan, X.; Peng, W.; Li, Y.; Zhang, G.; Zhang, F.; Fan, X. ACS Sustainable Chemistry & Engineering **2018,** 6 (5), 6388-6394.

16. Xu, J.; Liu, T.; Li, J.; Li, B.; Liu, Y.; Zhang, B.; Xiong, D.; Amorim, I.; Li, W.; Liu, L. Energy & Environmental Science **2018,** 11 (7), 1819-1827.

17. Zhou, W.; Jia, J.; Lu, J.; Yang, L.; Hou, D.; Li, G.; Chen, S. Nano Energy **2016,** 28, 29-43.

18. Xu, Y.; Li, Y.; Yin, S.; Yu, H.; Xue, H.; Li, X.; Wang, H.; Wang, L. Nanotechnology **2018,** 29 (22), 225403.

19. Mao, J.; He, C.-T.; Pei, J.; Chen, W.; He, D.; He, Y.; Zhuang, Z.; Chen, C.; Peng, Q.; Wang, D.; Li, Y. Nature Communications **2018,** 9 (1), 4958.

20. Ji, D.; Peng, L.; Shen, J.; Deng, M.; Mao, Z.; Tan, L.; Wang, M.; Xiang, R.; Wang, J.; Shah, S. S. A. Chemical Communications **2019,** 55 (22), 3290-3293.

21. Zhang, R.; Wang, X.; Yu, S.; Wen, T.; Zhu, X.; Yang, F.; Sun, X.; Wang, X.; Hu, W. Advanced Materials **2017,** 29 (9).

22. Wang, R.; Han, J.; Xu, P.; Gao, T.; Zhong, J.; Wang, X.; Zhang, X.; Li, Z.; Xu, L.; Song, B. Advanced Science **2020,** 7.

23. Kwon, I. S.; Kwak, I. H.; Ju, S.; Kang, S.; Han, S.; Park, Y. C.; Park, J.; Park, J. ACS Nano **2020,** 14 (9), 12184-12194.

24. Tang, C.; Cheng, N.; Pu, Z.; Xing, W.; Sun, X. Angewandte Chemie International Edition **2015,** 54 (32), 9351-9355.

25. He, Q.; Huang, S.; Liu, M.; Li, P.; Sun, W.; Hou, L. Inorganic Chemistry Frontiers **2020,** 7 (14), 2660-2668.

26. Pu, Z.; Amiinu, I. S.; Mu, S. Energy Technology **2016,** 4 (9), 1030-1034.

27. Hu, C.; Ma, Q.; Hung, S.-F.; Chen, Z.-N.; Ou, D.; Ren, B.; Chen, H. M.; Fu, G.; Zheng, N. Chem **2017,** 3 (1), 122-133.

28. Wang, X.; Li, W.; Xiong, D.; Petrovykh, D.; Liu, L. Advanced Functional Materials **2016,** 26.

29. Yan, J.; Huang, Y.; Zhang, L.; Zhou, M.; Yang, P.; Chen, W.; Deng, X.; Yang, H. Journal of Sol-Gel Science and Technology **2020,** 93 (2), 462-470.

30. Pu, Z.; Saana Amiinu, I.; Wang, M.; Yang, Y.; Mu, S. Nanoscale **2016,** 8 (16), 8500-4.

31. Zhao, Z.; Zhu, Z.; Wang, F.; Li, S.; Bao, X.; Zhang, L.; Lin, S.; Yang, Y. Chemical Engineering Journal **2021,** 415, 128885.

32. Yang, F.; Chen, Y.; Cheng, G.; Chen, S.; Luo, W. ACS Catalysis **2017,** 7 (6), 3824-3831.

33. Liu, X.; Gao, S.; Yang, P.; Wang, B.; Ou, J. Z.; Liu, Z.; Wang, Y. Applied Materials Today **2018,** 13, 158-165.